The tests of ElarmS presented here use data from past earthquakes. In a real-time implementation of ElarmS, the total processing time would be increased by data transmission times. Current TriNet stations are able to perform waveform processing on site. Because only parameter information is transmitted to central processing, transit time is reduced, allowing the processing of station information at the central site 1 s behind real time. The delay in transmitting the warning would be dependent on the technology used but could be reduced to less than 1 s. It is therefore conceivable to issue a ground-motion warning across southern California within 2 s of the times shown in Fig. 4B.

In conclusion, the implementation of ElarmS could provide a few to tens of seconds of warning to areas that may suffer structural damage in an earthquake. Buildings up to 60 km from the epicenter were red-tagged for demolition after the magnitude 6.7 Northridge earthquake. In a repeat event, occupants of buildings ~60 km from the epicenter could receive ~20 s of warning before peak ground motion. In a larger magnitude earthquake, the area damaged could be larger and even more warning time would be available to those further from the epicenter. For example, in the 1999 magnitude 7.6 Chi-Chi earthquake in Taiwan, many buildings were moderately damaged in the capital city of Taipei 145 km from the epicenter (18). With the ElarmS approach, there could be ~40 s of warning at a distance of 145 km.

The potential uses of a few to tens of seconds of warning span both personal and institutional preservation. Personal protective measures that could be undertaken at home and in the workplace include getting under desks and moving away from dangerous chemicals and machinery. During the response to a major earthquake, ElarmS could provide warning to rescue and clean-up personnel as they work on unstable debris. Institutional uses of short-term warnings include automated mass-transportation systems that can use a few seconds to slow and stop trains, abort airplane landings, and prevent additional cars from entering the freeway. Industry can shut down, or initiate the shutdown process of, sensitive equipment before peak ground motion arrives, preventing cascading failures. In addition to these immediate uses, the development of an early warning system will lead to the development of infrastructure that can use the information. For example, engineering companies in Japan are developing buildings with active response systems: The buildings can change their mechanical properties within a few seconds to better withstand ground motion (19).

References and Notes
1. A. Frankel et al., "National seismic hazard maps," Tech. Report No. Open-File Report 96-532 (U.S. Geological Survey, 1996).
2. H. Kanamori, E. Hauksson, T. Heaton, Nature 390, 461 (1997).
3. E. Hauksson et al., Seismol. Res. Lett. 72, 690 (2001).
4. H. Kanamori, E. Hauksson, T. Heaton, Eos 72, 564 (1991).
5. D. J. Wald et al., Earthquake Spectra 15, 537 (1999).
6. J. M. Espinosa Aranda et al., Seismol. Res. Lett. 66, 42 (1995).
7. J. Anderson et al., Seismol. Res. Lett. 66, 11 (1995).
8. Y. M. Wu, T. C. Shin, Y. B. Tsai, Bull. Seismol. Soc. Am. 88, 1254 (1998).
9. Y.-M. Wu, T.-L. Teng, Bull. Seismol. Soc. Am. 92, 2008 (2002).
10. Y. Nakamura, B. E. Tucker, Earthquakes Volcanoes 20, 140 (1988).
11. Y. Nakamura, B. E. Tucker, Calif. Geol., 41, 33 (1988).
12. Y. Nakamura, Proc. World Conf. Earthquake Eng. VII, 673 (1988).
13. N. M. Toksoz, A. M. Dainty, J. T. Bullitt, PAGEOPH 133, 475 (1990).
14. L. Jones et al., Science, 266, 389 (1994).
15. T. H. Heaton, Science 228, 987 (1985).
16. W. H. Bakun, F. G. Fischer, E. G. Jensen, J. Vanschaack, Bull. Seismol. Soc. Am. 84, 359 (1994).
17. Materials and methods are available as supporting material on Science Online.
18. Y. B. Tsai, T. M. Yu, H. L. Chao, C. P. Lee, Bull. Seismol. Soc. Am. 91, 1298 (2001).
19. G. W. Housner, L. A. Bergman, T. K. Caughey, A. G. Chassiakos, R. O. Claus, S.F. Masri, R. E. Skelton, T. T. Soong, B. F. Spencer, J. T. P. Yao, J. Eng. Mech. ASCE 123, 897 (1997).
20. We thank Y. Nakamura of Systems and Data Research Company, Japan, for discussions regarding UrEDAS, the Japanese earthquake early warning system; E. Hauksson and P. Small, both at the California Institute of Technology (Caltech), for their participation in discussions of the technical capabilities of TriNet; and two anonymous reviewers for their comments on this manuscript. Supported by the Seismological Laboratory at Caltech and the Graduate School of the University of Wisconsin–Madison.

Iron Partitioning in Earth's Mantle: Toward a Deep Lower Mantle Discontinuity

James Badro,[1] Guillaume Fiquet,[1] François Guyot,[1] Jean-Pascal Rueff,[2] Viktor V. Struzhkin,[3] György Vankó,[4] Giulio Monaco[4]

We measured the spin state of iron in ferropericlase ($Mg_{0.83}Fe_{0.17}$)O at high pressure and found a high-spin to low-spin transition occurring in the 60- to 70-gigapascal pressure range, corresponding to depths of 2000 kilometers in Earth's lower mantle. This transition implies that the partition coefficient of iron between ferropericlase and magnesium silicate perovskite, the two main constituents of the lower mantle, may increase by several orders of magnitude, depleting the perovskite phase of its iron. The lower mantle may then be composed of two different layers. The upper layer would consist of a phase mixture with about equal partitioning of iron between magnesium silicate perovskite and ferropericlase, whereas the lower layer would consist of almost iron-free perovskite and iron-rich ferropericlase. This stratification is likely to have profound implications for the transport properties of Earth's lowermost mantle.

Recent seismic observations (1) suggest that compositionally distinct domains exist in Earth's lower mantle, with a boundary located between 1700- and 2300-km depths. For these observations to be interpretable, the chemical and physical properties of the dominant phases in the lower mantle—namely $(Mg,Fe)SiO_3$ magnesium silicate perovskite (hereafter called perovskite) and $(Mg,Fe)O$ ferropericlase—must be determined at the pressure and temperature conditions of the deep mantle. In turn, these data can be fed into geochemical and geodynamical models (2, 3). The thermodynamic stability of perovskite at the pressure and temperature conditions of the lower mantle (4–9) indicates that it is stable to at least 2300 km depth (9). On the other hand, more subtle effects, driven by the chemistry of iron in the lower mantle, can affect the iron content in perovskite and ferropericlase; that is, they can affect the partition coefficient of iron between the two compounds. It has been suggested theoretically (10, 11) that iron in ferropericlase undergoes a high-spin (HS) to low-spin (LS) transition in the pressure domain of the lower mantle, and that iron in perovskite remains in

[1]Laboratoire de Minéralogie–Cristallographie de Paris, Université Paris VI, Université Paris 7, CNRS, IPGP, 4 place Jussieu, F-75252 Paris Cedex 05, France. [2]Laboratoire de Chimie Physique–Matière et Rayonnement (UMR 7614), Université Paris VI, 11 rue Pierre et Marie Curie, F-75231 Paris Cedex 05, France. [3]Geophysical Laboratory, Carnegie Institution of Washington, 5251 Broad Branch Road, N.W., Washington, DC 20015, USA. [4]European Synchrotron Radiation Facility (ESRF), B.P. 220, F-38043 Grenoble Cedex, France.

the HS state to pressures in excess of 1000 GPa (*12*). Such a change in the electronic properties of iron will alter the behavior of perovskite and ferropericlase as well as our current understanding of the lower mantle. Notably, the partition coefficient of iron between LS ferropericlase and HS perovskite would increase by several orders of magnitude, almost entirely depleting perovskite from its iron.

Here, we monitored the spin state and measured the spin magnetic moment of iron in $(Mg_{0.83} Fe_{0.17})O$ ferropericlase (*13*) as a function of pressure, from 0 to 80 GPa, by high-resolution Kβ x-ray emission spectroscopy. Initially in that process, a K shell electron absorbs an x-ray photon and is ejected from the atom (K edge absorption process), leaving a K shell core-hole. This is immediately followed by a series of radiative and nonradiative processes to recover the fundamental state. One of those is Kβ fluorescence or emission, which consists of a 3*p* electron collapsing onto the K shell, leading to a 3*p* core-hole final state. In transition metals, that 3*p* hole interacts strongly (via the exchange interaction) with the partially filled 3*d* shell. This interaction splits the final state into two main components that are identified in the emission spectrum as a main peak ($K\beta_{1,3}$) and a satellite peak (Kβ′). The strength of the exchange interaction depends mostly on *S* [the 3*d* local magnetic moment (total spin)], and the intensity of the satellite peak will depend on the spin polarization of the 3*d* shell (*14*). In turn, the emission line shape allows one to determine the magnetic spin

state of the 3*d* shell. The sensitivity of this technique to local spin magnetic moment has been established for transition-metal elements and their compounds (*15*–*17*) and has been applied to the study of pressure-induced HS-to-LS transitions (*18*–*20*). The emission spectrum of HS iron is characterized by a main peak $K\beta_{1,3}$, with an energy of 7058 eV, and a satellite peak Kβ′, located at lower energy as a result of the 3*p* core-hole–3*d* exchange interaction in the final state of the emission process. Because the LS state of ferrous iron is characterized by a spin magnetic moment equal to zero, the eventual collapse of the 3*d* magnetic moment as a consequence of pressure increase should lead to the disappearance of the low-energy satellite peak.

The measurements were performed on the ID16 inelastic x-ray scattering beamline of the European Synchrotron Radiation Facility (ESRF). The details of the experimental setup are reported in (*21*). The sample was loaded in an x-ray transparent gasket with a symmetrical Mao-Bell–type diamond anvil cell. Emission was excited through the diamonds with monochromatic x-ray radiation at 15 keV (*14*). The accumulation time for a spectrum was 6 hours. Emission was measured using the (531) reflection of a spherically bent silicon single-crystal analyzer. The spectra of the micrometer-sized samples were measured at different pressures (Fig. 1); the spectrum on a macroscopic sample at ambient pressure was measured outside the cell. The spectra show that there is a decrease of the satellite peak intensity at 49 GPa, and that it vanishes at 75 GPa, indicating a HS-to-LS tran-

sition in iron in ferropericlase between those pressures. Upon decompression, the spectrum at 64 GPa shows a partial reversal from HS to LS (a mixture of phases); at 41 GPa, the spectrum only shows the presence of the HS state (indicating a complete transformation).

Such a transition could radically alter the chemical behavior of ferropericlase and perovskite at high pressure. Although crystal-field theory calculations (*15, 22*) are not suitable for predicting HS-to-LS transitions (*12*), the scheme is sound for roughly estimating the electronic contributions to enthalpy and entropy of a HS or LS state, which in turn provides the free enthalpy change for the substitution reaction of Mg and Fe in perovskite and ferropericlase (*14*); at thermodynamic equilibrium, it is proportional to the logarithmic partition coefficient of iron between the two phases, given by

$$\ln(K) = \ln(Fe/Mg)_{mw} - \ln(Fe/Mg)_{pv}$$
$$= -(\Delta G/Nk_BT) \qquad (1)$$

Combining this qualitative energetic model with our observations, and taking into account the volume change and the electronic enthalpy and entropy changes between the HS and LS configurations (*14*), we see that the logarithmic partition coefficient of ferrous iron between ferropericlase and perovskite increases from around zero (about equal partitioning of iron between the two compounds) before the spin transition to around 10 to 14 after that transition, indicating that there is no ferrous iron in perovskite at thermodynamic equilibrium. If a subsequent HS-to-LS transition were to occur in perovskite, the partition coefficient would drop by four orders of magnitude (*14*) to values between 6 and 10. Therefore, at pressures greater then 70 GPa or at depths greater (*23*) than 2000 km, perovskite would then be completely iron-free, and any iron would be transferred into ferropericlase. More quantitative calculations based on quantum modeling of electronic interactions would be useful for refining this qualitative prediction.

Similar measurements on FeO (*19*) have shown that there is no transition to a LS state up to at least 143 GPa, which confirms the theoretical predictions that the transition pressure decreases with decreasing iron content (*16*). This trend complicates an analysis of iron partitioning in the mantle because as ferropericlase undergoes the spin transition, it is enriched in iron, as a consequence of which its transition point to the LS state is shifted to higher pressures and therefore to lower depths. This indicates that such a transition (and the depletion of iron from perovskite and simultaneous enrichment of ferropericlase) will be gradual and spread over a large range of depths rather than appear instantly, consistent with seismic observation of heterogeneities (*1*) rather than a sharp discontinu-
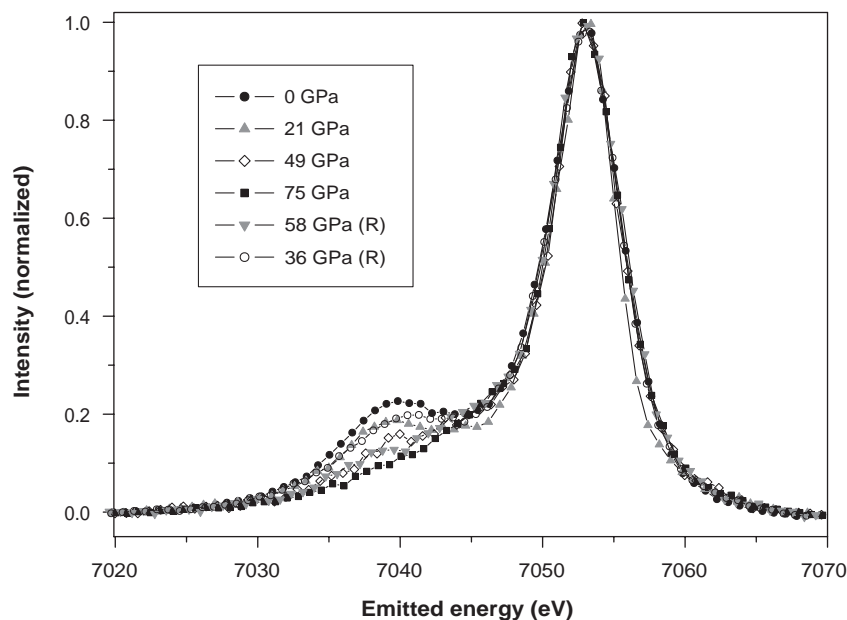
Fig. 1. X-ray emission spectra collected on ferropericlase $(Mg_{0.83}Fe_{0.17})O$ at different pressures. The presence of a satellite structure (Kβ′ line) on the low-energy side of the iron main emission line ($K\beta_{1,3}$ line) is characteristic of a HS 3*d* magnetic moment. This structure collapses at high pressure upon compression and then reforms upon pressure decrease [spectra with (R)]. The system is in the HS state at 36 GPa, in a HS-LS mixture at 49 and 58 GPa, and in the LS state at 75 GPa. The pure LS component appears between 58 and 75 GPa.

ity. The transition could thus be accompanied by phase separation between iron-rich HS and magnesium-rich LS ferropericlases. This could explain x-ray diffraction observations suggesting a breakdown of ferropericlase (24), which were observed in the same pressure range as our spin transition.

The observed transitions indicate that the lower mantle would be segregated into two different layers characterized by different iron partitioning between perovskite and ferroperi-clase. The transition pressures are consistent with the depths at which lower mantle layering has been proposed (1) and provide a mineral physics basis for an Earth's lower mantle made of two distinct layers. Moreover, observations that the iron-free olivine (forsterite) is more viscous than iron-bearing phases (25, 26) imply that, similarly, an iron-free perovskite is likely to be more viscous than an iron-rich one. This idea is also corroborated by the fact that viscosity scales in many materials (27) with T/T_m (the ratio of temperature to melting temperature) and that the melting point of an iron-free perovskite is much higher than that of an iron-bearing one (28, 29). In that sense, because perovskite is the major lower-mantle phase, the transition could have a fairly strong rheological signature as inferred from geophysical observations (30) and could affect the geodynamics in the lowermost mantle. Further studies could constrain geodynamical interpretations (2, 3) of the seismic observations and could enable quantification of the effect of such a viscous layer on the dynamics of plumes. Note that such a layering model requires no isolated convection cells, because the chemistry of the two layers is reversible as a function of depth (the transition is reversible upon decompression); uplifted materials will recover the partitioning properties of the top layer.

Iron-free perovskite is stable to very high pressures and temperatures. It was speculated that the breakdown of iron-bearing perovskite (6) at the core-mantle boundary (CMB) was responsible for the chemical heterogeneities observed in the D'' layer. We suggest, however, that the iron-free end member is the one that is most likely to be present at those depths, and that the interaction of iron-rich ferropericlase with the liquid outer core should instead be taken into consideration. Geodynamical modeling of this lowermost layer could contribute to our understanding of core-mantle interactions because dominant iron-depleted perovskite could create an electrically, thermally (31), and rheologically insulating lid above the CMB.

References and Notes
1. R. van der Hilst, S. Kárason, *Science* **283**, 1885 (1999).
2. T. Lay, Q. Williams, E. J. Garnero, *Nature* **392**, 461 (1998).
3. L. H. Kellogg, B. H. Hager, R. D. van der Hilst, *Science* **283**, 1881 (1999).
4. E. Knittle, R. Jeanloz, *Science* **235**, 668 (1987).
5. S. E. Kesson, J. D. Fitz Gerald, J. M. Shelly, *Nature* **393**, 253 (1998).
6. G. Serghiou, A. Zerr, R. Boehler, *Science* **280**, 2093 (1998).
7. G. Fiquet *et al.*, *Geophys. Res. Lett.* **27**, 21 (2000).
8. D. Andrault, *J. Geophys. Res.* **106**, 2079 (2001).
9. S.-H. Shim, T. S. Duffy, G. Shen, *Science* **292**, 2437 (2001).
10. D. M. Shermann, *J. Geophys. Res.* **96**, 14299 (1991).
11. J. Brodholt, unpublished data.
12. R. E. Cohen, I. I. Mazin, D. G. Isaak, *Science* **275**, 654 (1997).
13. The sample $(Mg_{0.83}Fe_{0.17})O$ was prepared by annealing of a mixture of MgO and Fe_2O_3 maintained at 1673 K for 24 hours under a controlled oxygen fugacity between 10^{-9} and 10^{-11} atm. These samples were characterized by x-ray diffraction and shown to be pure ferropericlase.
14. See supporting data on *Science* Online.
15. G. Peng *et al.*, *Appl. Phys. Lett.* **65**, 2527 (1994).
16. F. M. F. de Groot *et al.*, *Phys. Rev. B* **51**, 1045 (1995).
17. X. Wang *et al.*, *Phys. Rev. B* **56**, 4553 (1997).
18. J.-P. Rueff *et al.*, *Phys. Rev. Lett.* **82**, 3284 (1999).
19. J. Badro *et al.*, *Phys. Rev. Lett.* **83**, 4101 (1999).
20. J.-P. Rueff *et al.*, *Phys. Rev. B* **60**, 14510 (1999).
21. F. Sette *et al.*, *Phys. Rev. Lett.* **75**, 850 (1995).
22. V. Malavergne, F. Guyot, Y. Wang, I. Martinez, *Earth Planet. Sci. Lett.* **146**, 499 (1997).
23. The critical parameter for this type of transition is density; in the absence of structural phase transitions, the effect of temperature is to increase the transition pressure to compensate for the thermal expansion. It is therefore not possible to express precisely the transition pressures in terms of depths within Earth, because the thermal expansion coefficient at those pressures is not known.
24. L. Dubrovinsky *et al.*, *Eur. J. Mineral.* **13**, 857 (2001).
25. W. B. Durham, C. Goetze, *J. Geophys. Res.* **82**, 5737 (1977).
26. W. B. Durham, C. Froideveaux, O. Jaoul, *Phys. Earth Planet. Inter.* **19**, 263 (1979).
27. J. Weertman, J. R. Weertman, *Annu. Rev. Geophys.* **3**, 293 (1975).
28. P. E. van Keken, D. A. Yuen, A. P. van den Berg, *J. Geophys. Res.* **100**, 15233 (1995).
29. A. Zerr, R. Boehler, *Science* **262**, 553 (1993).
30. V. Corrieu, C. Thoraval, Y. Ricard, *Geophys. J. Int.* **120**, 516 (1995).
31. LS ferropericlase is a much better radiative thermal conductor than HS ferropericlase (10) because it is transparent to thermal radiation in the near-infrared.

Diverse Plant and Animal Genetic Records from Holocene and Pleistocene Sediments

Eske Willerslev,[1]* Anders J. Hansen,[1]*† Jonas Binladen,[1] Tina B. Brand,[1] M. Thomas P. Gilbert,[2] Beth Shapiro,[2] Michael Bunce,[2] Carsten Wiuf,[3] David A. Gilichinsky,[4] Alan Cooper[2]

Genetic analyses of permafrost and temperate sediments reveal that plant and animal DNA may be preserved for long periods, even in the absence of obvious macrofossils. In Siberia, five permafrost cores ranging from 400,000 to 10,000 years old contained at least 19 different plant taxa, including the oldest authenticated ancient DNA sequences known, and megafaunal sequences including mammoth, bison, and horse. The genetic data record a number of dramatic changes in the taxonomic diversity and composition of Beringian vegetation and fauna. Temperate cave sediments in New Zealand also yielded DNA sequences of extinct biota, including two species of ratite moa, and 29 plant taxa characteristic of the prehuman environment. Therefore, many sedimentary deposits may contain unique, and widespread, genetic records of paleoenvironments.

Most authenticated ancient DNA studies (1) have analyzed hard or soft tissue remains of flora and fauna from the late Pleistocene [∼100 to 10 ky (thousand years)] or Holocene (past 10 ky). Preserved genetic information has provided unique insights into many evolutionary and ecological processes (2–6) and also provides an important test of methods for reconstructing past events (7–9). However, a broader utility for ancient DNA studies has been prevented by experimental difficulties (1, 10) and the rarity of suitable fossilization. Even in areas with excellent ancient DNA preservation and large numbers of specimens, such as Beringia (the late Pleistocene ice-free refugium that stretched from northeast Siberia across the exposed Bering land bridge to western Canada), it has been possible to obtain only limited paleoenvironmental views (3). Consequently, we exam-

[1]Department of Evolutionary Biology, Zoological Institute, University of Copenhagen, Universitetsparken 15, Denmark DK-2100 Ø. [2]Henry Wellcome Ancient Biomolecules Centre, Department of Zoology, University of Oxford, Oxford OX1 3PS, UK. [3]Department of Statistics, University of Oxford, 1 South Parks Road, Oxford OX1 3TG, UK. [4]Soil Cryology Laboratory, Institute for PhysicoChemical and Biological Problems in Soil Science, Russian Academy of Sciences, 142290, Pushchino, Moscow Region, Russia.

*These authors contributed equally to this work.
†To whom correspondence should be addressed. E-mail: ajhansen@zi.ku.dk